Rainfall Analysis of the May 2021 Southeastern Texas and Southern Louisiana Flood

Vincent M. Brown[a], Alan W. Black[b], Douglas M. Hultstrand[c], William D. Kappel[c], Derek T. Thompson[a], Alicia M. Bentley[d], Anna K. Sitzman[a], Barry D. Keim[a]

[a] *Department of Geography and Anthropology, Louisiana State University, Baton Rouge, LA, USA*

[b] *Department of Geography and Geographic Information Sciences, Southern Illinois University-Edwardsville, Edwardsville, IL, USA.*

[c] *Applied Weather Associates, Monument, CO, USA*

[d] *Department of Atmospheric and Environmental Sciences, University at Albany, State University of New York, Albany, NY, United States*

Corresponding author: Vincent Brown (vbrow31@lsu.edu)

E235 Howe-Russell-Kniffen Geoscience Complex

Baton Rouge, LA 70803

Key Words: Extreme Precipitation, Depth-Area-Duration, Average Recurrence Interval

ABSTRACT

This paper analyzes the heavy rainfall on 16–20 May 2021 across southeastern Texas and southern Louisiana. In Louisiana, five fatalities were attributed to the event and > $1 billion in losses. The rainfall was caused by two slow-moving, mesoscale convective vortices that concentrated precipitation south of Port Arthur, TX, Lake Charles, LA, and Baton Rouge, LA, in 6 to 12-hour periods. Using calibrated radar data, the Storm Precipitation Analysis System estimated 6-h rainfall totals of 254–362 mm south of Lake Charles, surpassing 200–500-year average recurrence intervals (ARI) for those locations, with an isolated area receiving 367.5 mm, equating to a > 800-year ARI. In East Baton Rouge Parish, LA, 203–268 mm was estimated in 6-h (200–500-year ARI), with an isolated area receiving 274 mm, equivalent to a 750-year ARI. A comparison of the May 2021 and August 2016 events, which both affected southern Louisiana, is made using a depth-area-duration analysis. While the forcing mechanisms differed, 1–6 h rainfall depths were similar at 1–25,900 km^2. The May 2021 event exceeded rainfall depths produced by the August 2016 event for 2–6 h durations for area sizes of 1–388 km^2, highlighting the precipitation intensity produced by the May 2021 event.

1. Introduction

The northern Gulf of Mexico Coast frequently experiences extreme precipitation events that produce widespread flooding and incur damages ≥ $1 billion. These events are often induced by named tropical cyclones or systems that have discernable tropical characteristics (e.g., instability through deep, tropically moist layers). Recent examples include Southern Louisiana in 2016, where > 864 mm (34 in.) of precipitation fell in 4 days (Brown et al., 2020a), Hurricane Harvey in 2017, where > 1270 mm (50 in.) occurred in 5 days near Houston, TX (Kappel and Hultstrand, 2018), and Tropical Storm Imelda in 2019, where numerous sites near Beaumont, TX recorded > 1016 mm (40 in.) in 3 days (Latto and Berg, 2020). While most billion-dollar flood events receive extensive media coverage, a lesser-known, non-tropical, extreme precipitation event from 16–20 May 2021 produced > 483 mm (19 in.) of rain near Port Arthur, TX, and Lake Charles, LA, and > 356 mm (14 in.) near Baton Rouge, LA (Fig 1), with many locations experiencing 50–70% of the storm total in just 6-h.

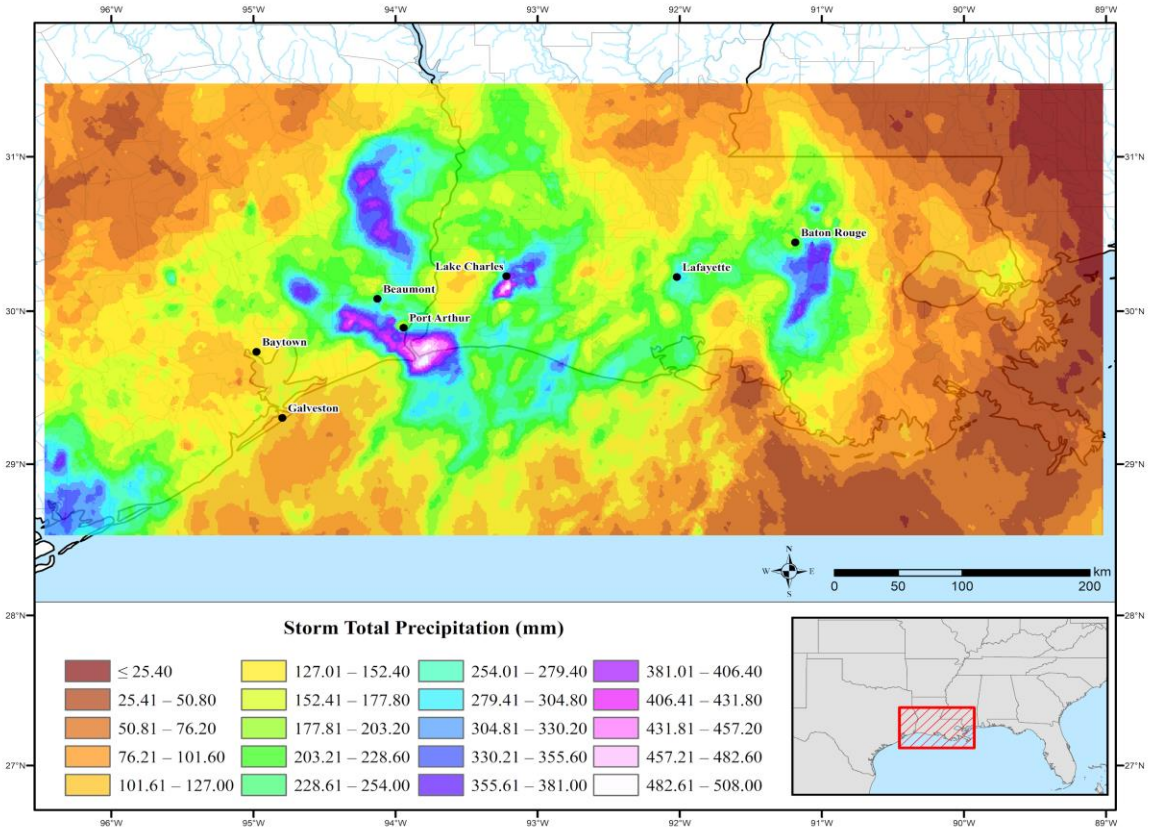

Fig 1. Storm total isohyets generated by the Storm Precipitation Analysis System (SPAS) across southeastern Texas and southern Louisiana during 01 UTC 16 May–00 UTC 21 May.

According to the Louisiana Department of Health, five fatalities were directly attributed to the flooding, with three in submerged vehicles (Louisiana Department of Health, Personal Communication 2 Feb 2023). In Baton Rouge, LA, roughly 16,000 residents were without power immediately following the storm, and nearly 50 roadways were impassable, including a section of Interstate 10 (Brackett, 2021). The Baton Rouge Fire Department rescued > 200 people, and the St. George Fire Department (also in Baton Rouge, LA) conducted 81 high-water rescues (WAFB, 2021). Over 250 people were evacuated by school bus to East Baton Rouge Parish shelters. Over 2,700 homes in Ascension, Calcasieu, East Baton Rouge, Iberville, and Lafayette parishes were damaged, of which six were destroyed and 703 sustained major damage (Davies, 2021). In Lake Charles, LA, which was still recovering from Hurricanes Laura (August 2020) and Delta (October 2020), an estimated 400–500 homes were lost due to flooding. Over 100 rescue calls were placed in Lake Charles on 17 May 2021 from motorists caught off guard and stranded/flooded during the peak rainfall (Lynch, 2021). On 28 May 2021, a federal disaster declaration was requested for Louisiana, and on 2 June 2021, it was approved, covering the parishes of Ascension, Calcasieu, East Baton Rouge, Iberville, and Lafayette.

The synoptic setting of the event was not particularly indicative of a significant flash flood event; thus, there was no advance warning to inform residents of the potential risk. The National Weather Service (NWS) quantitative precipitation forecast (QPF) on the day before and the morning of the event underestimated the areal average rainfall across the region. The QPF issued at 2046 UTC 16 May 2021, covering 00 UTC 17 May–00 UTC 18 May 2021 (24-h), when most of the rainfall transpired in Port Arthur, TX, and Lake Charles, LA, estimated 12.7–25.4 mm (0.5–1.0 in) for the affected area, with isolated locations expected to receive ~38.1 mm (1.5 in). The 24-h QPF issued at 0849 UTC 17 May 2021 (12 UTC 17 May–12 UTC 18 May 2021), a period when most of the rain occurred near Baton Rouge, LA, again estimated 12.7–25.4 mm (0.5–1.0 in) for areas surrounding Baton Rouge, LA, with isolated locations expected to receive ~38.1 mm (1.5 in). Additionally, the flood warnings in the Lake Charles, LA area were issued around mid-morning (1510 UTC 17 May 2023), after many residents had left their homes for the day.

As discussed in prior studies (e.g., Min et al., 2011; Trenberth, 2011; Lehmann et al., 2015; Easterling et al., 2017; Trenberth et al., 2018; Brown et al., 2020b; etc.), the frequency and

intensity of recent precipitation events, combined with the resulting floods, have raised questions about the effect of global climate change on extreme precipitation climatology. Recent research and assessments have discovered changes in precipitation characteristics across the U.S. (Easterling et al., 2017; Kunkel et al., 2020; Seneviratne et al., 2021). For example, Skeeter et al. (2019) found that intense precipitation events (99th percentile daily/multiday events) increased in frequency and intensity across the southeastern U.S. from 1950–2016. More specifically, Prein et al. (2017) noted that mesoscale convective systems (MCS) have increased in frequency and intensity during the warm season from 1979–2014; however, the significant trends were farther north of the U.S. Gulf Coast (excluding parts of Florida). Kunkel et al. (2020) showed that extreme daily precipitation events positively correlate with precipitable water, demonstrating that elevated precipitable water and its convergence are important factors in the observed changes in extreme precipitation events. As the climate warms, the atmosphere's water vapor capacity increases (see Trenberth 2011), and the concentration of water vapor in the atmosphere rises (known as the water vapor feedback, Forster et al., 2021). The combination of these factors has contributed to the observed upward trends in extreme precipitation events (Kunkel et al., 2020) and may continue to play a role in the future (Seneviratne et al., 2021), potentially leading to more frequent extreme rainfall, assuming no change in forcing mechanisms or moisture limitations. Thus, it is important to understand the characteristics of extreme precipitation (e.g., precipitable water, intensity, duration, etc.) events to identify common factors and forcing mechanisms.

The 16–20 May 2021 event is yet another extreme rainfall event in successive years across the Southeast U.S. For example, Charleston, SC, in 2015 (> 710 mm in 4 days; Kappel et al., 2015), Baton Rouge, LA, in 2016 (> 864 mm in 4 days; Brown et al., 2020a), Houston, TX, in 2017 (> 1270 mm in 5 days; Kappel and Hultstrand, 2018), Elizabethtown, NC in 2018 (>1116 mm in 4 days; Kappel et al., 2019), Beaumont, TX in 2019 (> 1016 mm in 3 days; Latto and Berg, 2020), Pembroke Pines, FL in 2020 (> 508 mm in 3 days; Pasch et al., 2021), and Fort Lauderdale, FL in 2023 (> 650 mm in 1 day; NCEI, 2023). This research is part of a growing collection of case studies focusing on heavy and extreme rainfall events across the U.S. (see Brown et al., 2020a, for a detailed list of events). The goal of this work is to examine the 16–20 May 2021 event from both a meteorological and climatological perspective by assessing the synoptic setting of the event, quantifying the spatiotemporal pattern of rainfall, and placing the

storm in a historical context using average return intervals (ARIs). A comparison is also drawn between the August 2016 Southern Louisiana event, which affected similar areas of south Louisiana, using a depth–area–duration (DAD) analysis.

The specific research questions of this study are

1. Where did the rainfall center(s) occur and how much precipitation accumulated?
2. What were the average recurrence intervals of the rainfall, specifically at the 6-h and 24-h duration?
3. How does the May 2021 event compare to August 2016 event at specific area sizes and durations?

The following sections describe the data and methods, discuss the synoptic characteristics of the event, and assess the spatiotemporal pattern of rainfall associated with this event.

2. Data and Methods

The Storm Precipitation Analysis System (SPAS; Parzybok and Tomlinson, 2006; Hultstrand and Kappel, 2017) was used to assess the spatiotemporal rainfall pattern of the 16–20 May 2021 event. SPAS is a gridded rainfall analysis software package that incorporates all available rainfall data, including rain gauges, supplemental/bucket survey rainfall, dynamically calibrated NEXRAD radar, and climatological base maps (e.g., PRISM Climate Group, 2021) to produce a precise representation of accumulated rainfall in both space and time across the event domain. Rainfall estimates are produced at intervals as short as 5 minutes and spatial scales as fine as 1 km^2. One advantage of the SPAS process is that it does not apply a standard radar reflectivity factor (Z) to the rainfall rate (R) for an entire storm. Instead, SPAS uses a least square fitting procedure for optimizing the Z-R relationship during each hour of the storm. The process aggregates 5-minute NEXRAD reflectivity (Z) and relates it to gauged-based hourly precipitation (R) to establish the best fit for that hour. SPAS was originally developed for probable maximum precipitation (PMP) analysis and hydrologic model calibration based on National Oceanic and Atmospheric Administration (NOAA) Hydrometeorological Report storm analysis methodologies using similar methods for NWS Stage IV (Du, 2011) and Multi-Radar Multi-Sensor (MRMS) but can also be used to reconstruct precipitation events (e.g., Brown et

al., 2020a). SPAS has been used in numerous technical reports (e.g., Kappel et al., 2021a, 2021b, 2023) and rainfall research (Mahoney et al., 2021; Keim et al., 2018; Brown et al., 2020a). Additional information on the SPAS system is available in Parzybok and Tomlinson (2006), Hultstrand and Kappel (2017), Keim et al., (2018), Brown et al., (2020a), and Mahoney et al. (2021). Here, we use SPAS to generate storm total, maximum 6- and 24-h precipitation, and ARIs at each gridded location for the precipitation period of the event, which was defined as 01 UTC 16 May–00 UTC 21 May (120 h). This period was selected because it represents a dry-to-dry period bounding the rainfall of interest for most of the domain and precipitation centers.

ARIs indicate the average time between events of a given magnitude when averaged over a long period (Lincoln et al., 2017) and are calculated for an event for a range of different durations, typically from hours to days. Derived ARIs used are from NOAA Atlas 14 (Perica et al., 2013), which contains rainfall durations ranging from five minutes to 60 days with recurrence intervals extending from 1–1000 years. NWS gridded point precipitation estimates (derived from Stage IV) are often used to place rainfall in a historical context using NOAA Atlas 14 (e.g., https://www.weather.gov/owp/hdsc_aep); however, SPAS can also be used because it implements gridded point precipitation estimates, based on gauge data and radar adjustments, to compare to NOAA Atlas 14-point precipitation frequency estimates. Finally, it is important to note that as the duration and ARIs increase, the confidence interval widths of a given ARI estimate also increase, resulting from variability in precipitation and the rare nature of extreme events (Brown et al., 2020a).

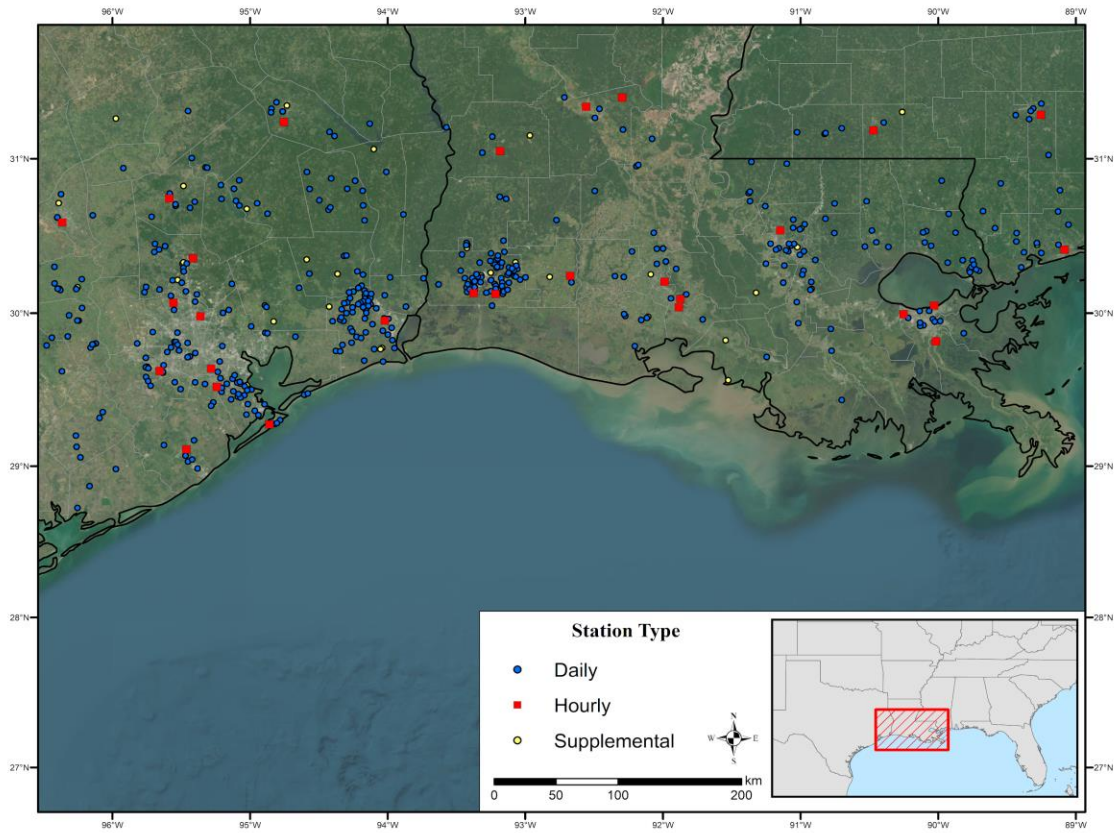

Fig 2. Station locations across the storm domain. Hourly stations (n=28) are denoted by red squares, daily stations (n=418) are denoted by blue circles, and supplemental stations (n=36) are denoted by yellow circles.

A total of 482 *in-situ* rainfall sites were input into SPAS to quantify the rainfall (Fig 2). Of these, 28 contained hourly data to help temporally distribute the rainfall, and 418 contained complete daily data (e.g., daily totals from 16–20 May). An additional 36 stations were input as supplemental stations. Most supplemental stations contained multi-day accumulations or differing/unknown daily observation times but were still useful for total storm information. The 482 stations come from six different sources or networks, Automated Weather Observing Systems or AWOS (two stations), Weather-Bureau-Army-Navy or WBAN (31 stations), Cooperative Observer Network or COOP (79 stations), Community Collaborative Rain, Hail, & Snow Network or CoCoRaHS (254 stations), Calcasieu Parish Police Jury's Alert System - One Rain (58 stations), and Jefferson County (Texas) Drainage District No.6 - One Rain (58 stations). To further help temporally distribute precipitation and to improve the interpolation of precipitation estimates between stations, 5-minute NEXRAD (Level II) Base Reflectivity

Mosaics were acquired from Iowa State University (IEM) from 01 UTC 16 May–00 UTC 21 May (120 h).

To quantify the magnitude and extent of the precipitation, DAD tables and mass curves were generated using SPAS. DAD analysis enables objective characterization of storm precipitation since using gauge information or radar alone does not provide insight into a storm's areal effects (Parzybok et al., 2009). This type of analysis is also important for evaluating hydrological effects because it estimates the volume of precipitation that fell over various area sizes during the storm. It also enables comparisons between events at specific area sizes (e.g., 100 km^2) and durations (e.g., 24-h). Two non-overlapping zones were delineated in this analysis because the storm produced two distinct precipitation maxima that varied in time and space (Fig 3). Zone 1 encompasses Beaumont, TX, Lake Charles, LA, and other areas affected by the storm ~12 hours earlier than locations in Zone 2, i.e., Baton Rouge, LA. Producing one DAD Zone for the entire storm would have co-joined the two distinct precipitation maxima, creating an unrealistic characterization of the spatial extent and temporal variation of the heaviest rain.

Finally, numerous NWS products from the Weather Prediction Center, such as the Mesoscale Precipitation Discussion, Excessive Rainfall Outlook, and QPFs, were reviewed in detail to describe the meteorology of the event. Additionally, synoptic scale 0.25° Global Forecast System (GFS) analyses (during forecast hour zero) were used to describe the event and create a figure of 500-hPa geopotential height, temperature, ascent, cyclonic relative vorticity, and wind.

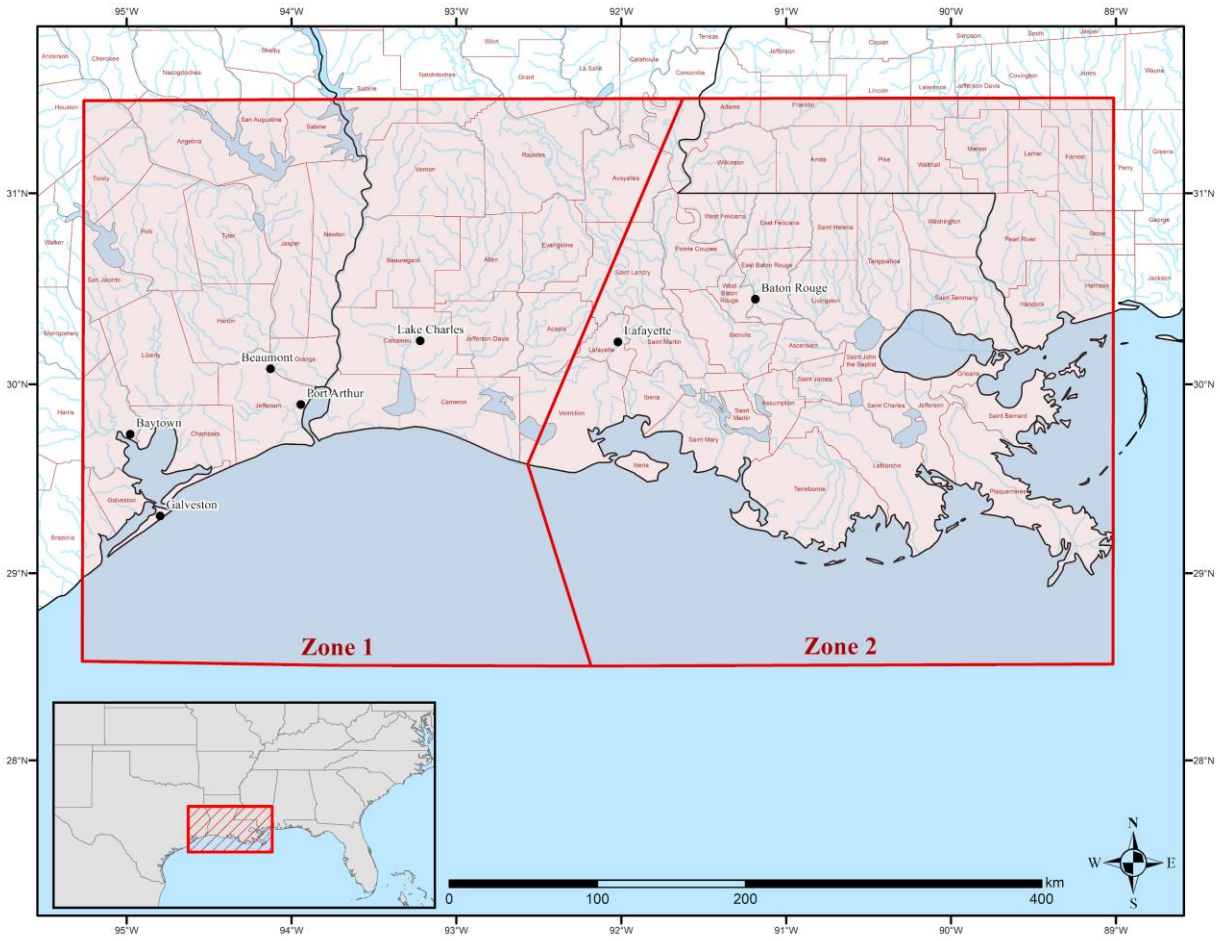

Fig 3. Delineated zones used for mass curves and DAD analysis for the May 2021 storm.

3. Results

a. Meteorological Summary

The extreme rainfall totals observed during the 16–20 May 2021 event resulted from two slow-moving mesoscale convective vortices (MCV) which arose from thunderstorms that began in western Texas and eastern New Mexico on 15 May 2021 along a surface dryline and ahead of a shortwave trough. The shortwave trough and subsequent cutoff low created a favorable region for mid-level ascent over Louisiana for several days (Fig 4), while weak winds aloft resulted in less than 15 m/s (30 kts) of effective shear, yielding outflow-dominant multicell thunderstorms in the region. Figure 4 shows the cutoff low at 500 hPa with cyclonic relative vorticity and

associated mid-level ascent moving west to east from 15–20 May 2021, which aided and sustained thunderstorm activity across southeastern Texas and southern Louisiana.

By 00 UTC on 16 May, a large area of thunderstorm activity extended from the Big Bend region of Texas northward to the Oklahoma panhandle. This activity weakened as it moved east with the loss of diurnal heating, resulting in two MCVs by 12 UTC on 16 May. The northernmost MCV was located near Wichita Falls, TX, while the other was located over the Texas Hill Country. By 18 UTC on 16 May, these features continued to drift slowly eastward and were located over central Oklahoma and the Texas coastal plain. Ahead of the MCVs, southerly winds through a relatively deep layer of the near-surface troposphere resulted in the advection of ample moisture into the study region as they moved east. By 02 UTC on 17 May, the southernmost of the original two MCVs was located near Houston, TX. Thunderstorms that formed during the day on 16 May associated with this feature led to the formation of a new MCV. This new MCV was located over the Gulf of Mexico to the south of Galveston, TX. The combined influence of these two MCVs enhanced southerly low-level flow and moisture advection from the Gulf of Mexico, like what had occurred the day before across parts of Oklahoma and the Texas coastal plain.

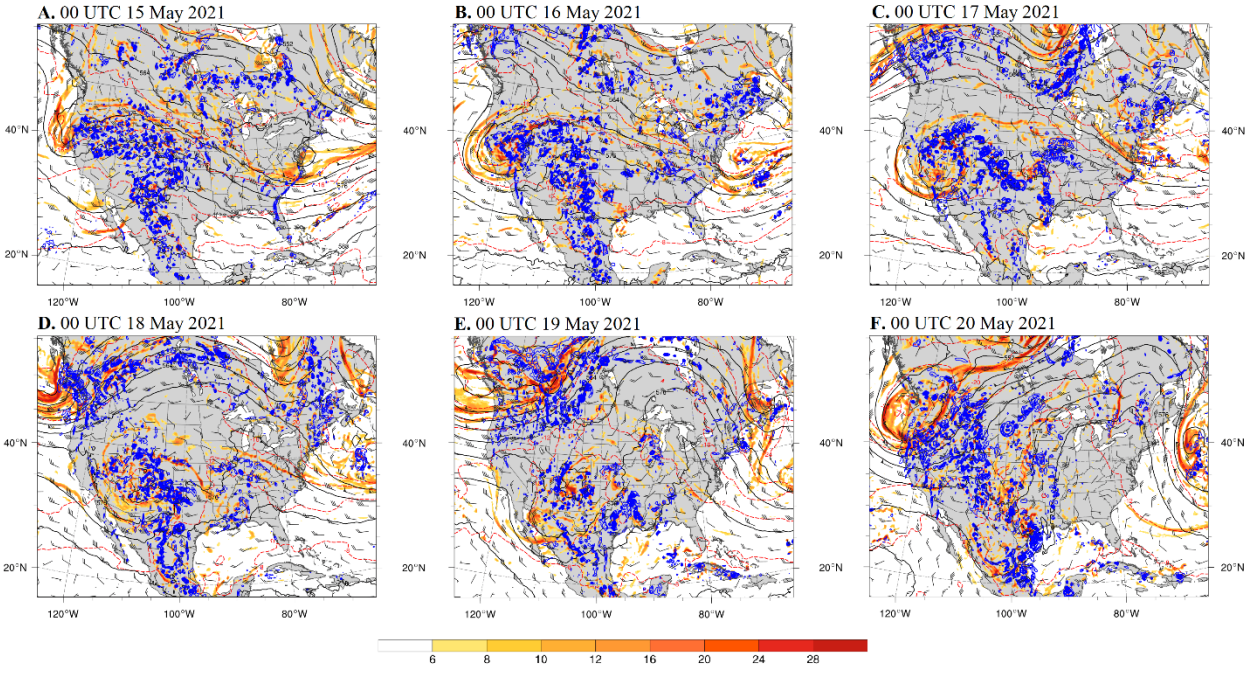

Fig 4. 500-hPa geopotential height (black contours, dam), 500-hPa temperature (red contours, °C), 500-hPa ascent (blue contours, 5 x 10^{-3} hPa/s), 500-hPa cyclonic relative vorticity (x 10^{-5} s^{-1}), and 500-hPa wind (barbs, kt) for (A) 00 UTC 15 May 2021, (B) 00 UTC 16 May 2021, (C) 00 UTC 17 May 2021, (D) 00 UTC 18 May 2021, (E) 00 UTC 19 May 2021, and (F) 00 UTC 20 May 2021.

As the MCV over the Gulf of Mexico moved east, precipitation spread across southeast Texas (Port Arthur, TX) and southwest Louisiana (Lake Charles, LA). The circulation around the MCV resulted in individual thunderstorms moving south to north, training over the same locations. The heaviest precipitation in Port Arthur, TX/Lake Charles, LA, began around 12 UTC on 17 May. Sounding data from Lake Charles at 12 UTC on 17 May (Fig 5) reveals a nearly saturated atmosphere from the surface through approximately 800 hPa (Fig 5a.) below a drier elevated mixed layer (Fig 5b.), resulting in convective available potential energy (CAPE; Fig 5c.) of 629 J/kg and a convective inhibition (CIN) of -15.6 J/kg (Fig 5d.). In addition, southeast winds of around 7–8 m/s (15 kts) at the surface with stronger southerly winds of around 18 m/s (35 kts) in a layer from approximately 1000–900 hPa (300–1200m AGL; Fig 5e.) continued to advect moisture into the region. This resulted in precipitable water values measured from the sounding of 45.45 mm (1.79 in; Fig 5f.), a value above the 90th percentile of 43.94 mm (1.73 in) according to the Storm Prediction Center's Sounding Climatology (https://www.spc.noaa.gov/exper/soundingclimov2/). Precipitable water values are an important factor for rainfall accumulation (Kelsey et al., 2022) and heavy rainfall (Wang et al., 2017), and were elevated due to the advection of moisture from the Gulf of Mexico preceding the event. Sea surface temperatures (SSTs) along the Texas and Louisiana coast and offshore were between 23–27°C (National Centers for Environmental Information, Optimum Interpolation SST) from 1–17 May 2023, which, in some areas, were 1–3°C above the 1981–2011 climatological average and likely enhanced atmospheric water vapor.

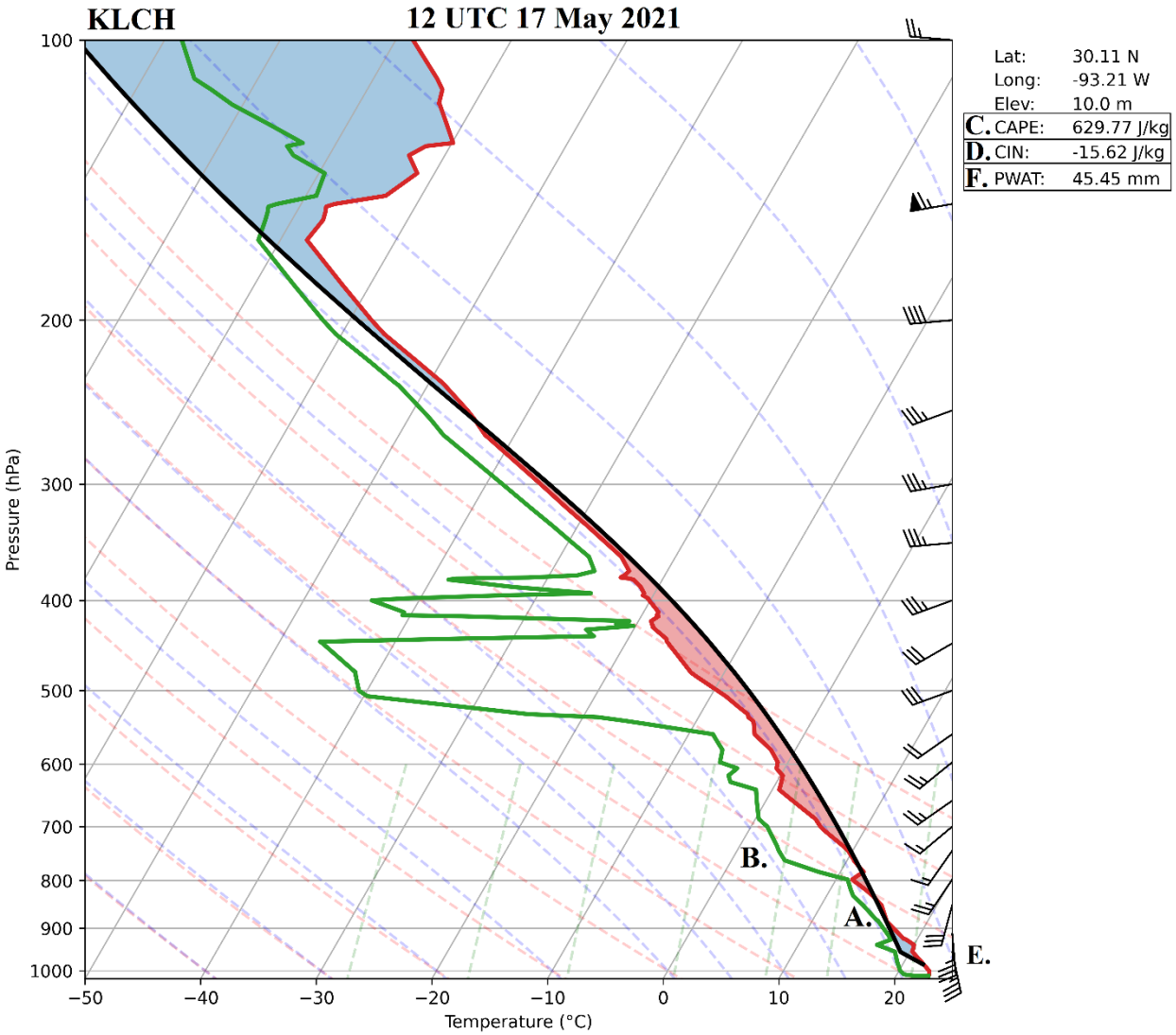

Fig 5. Skew-*T* from Lake Charles, LA (KLCH) at 12 UTC 17 May 2021. Created using MetPy v1.5.

This story would be repeated as the MCV moved farther east. The MCV offshore and the most intense precipitation continued eastward across the study area during the day on 17 May. The heaviest precipitation across southeast Louisiana (e.g., Baton Rouge, LA) began around 22 UTC on 17 May. An environment like what was observed earlier in the day at Lake Charles, LA, was sampled by the 00 UTC 18 May 2021 sounding from Slidell, LA (Fig 6). A veering wind profile (southeast-to-southwest winds) was observed from the surface through around ~750 hPa (2200 m AGL; Fig 6a), bringing moisture from the Gulf of Mexico into the region with CAPE of

581 J/kg (Fig 6b) and -2.87 J/kg of CIN (Fig 6c). The precipitable water value of 43.89 mm (1.72 in; Fig 6d) measured from the Slidell sounding was near the 90th percentile (43.94 mm, 1.73 in) for that day. Precipitation continued near Baton Rouge, LA, through ~12 UTC on 18 May when the MCV moved east of the area.

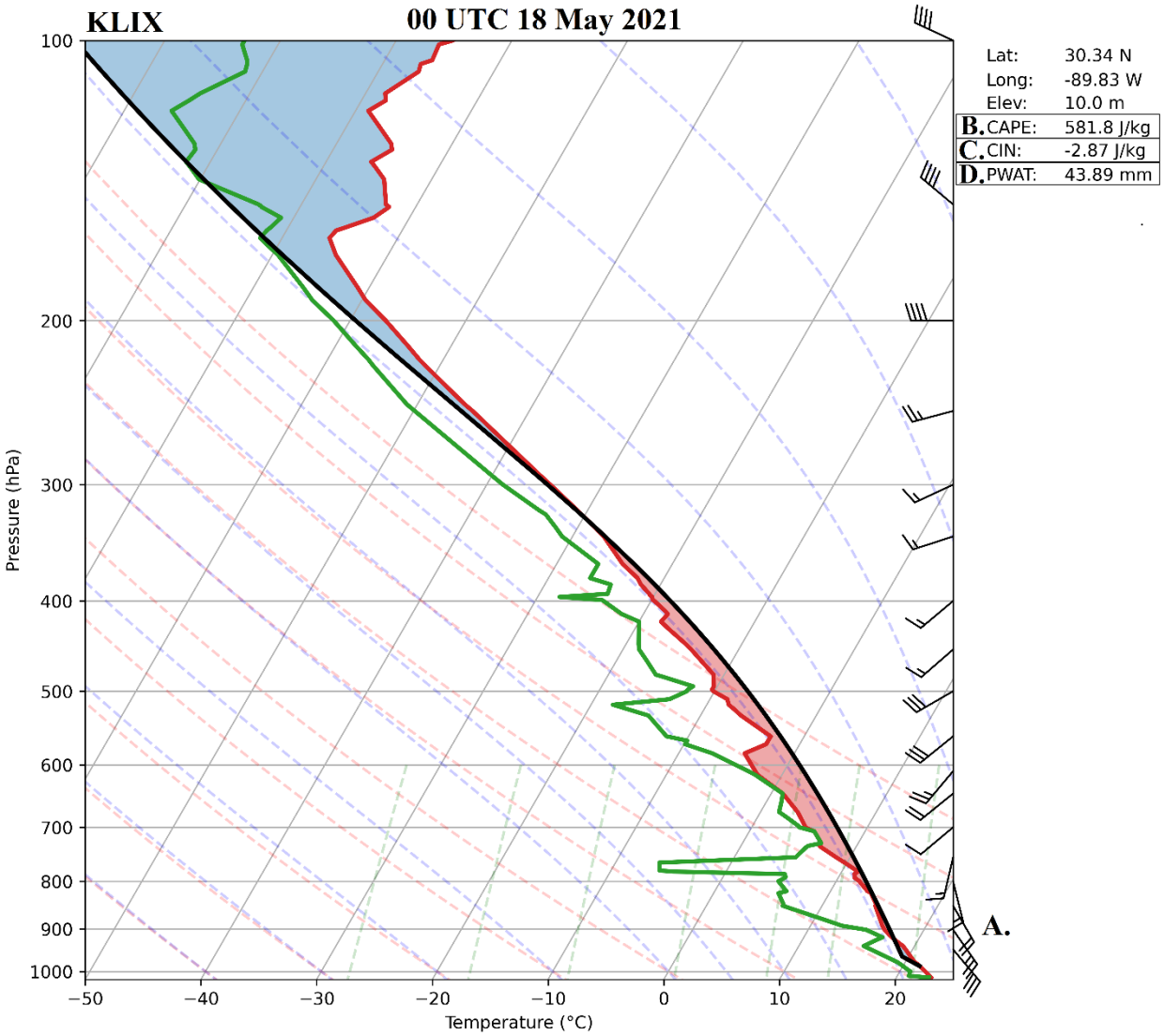

Fig 6. Same as Fig 5 except for Slidell, LA (KLIX) at 00 UTC 18 May 2021.

b. Hourly Rainfall

1. Hourly Observations

Hourly rainfall data were investigated at 28 stations within the storm domain. Observations from those stations, excluding traces, were examined from 16–20 May 2021 (Table 1). The heaviest hourly rainfall observation between the stations was 77.98 mm (3.07 in.), recorded at Lake Charles Regional Airport (KLCH) for the hour ending at 18 UTC (1:00 pm LST) on 17 May 2021. This hourly observation is less than (but within the 90% confidence interval of) the estimated 10-yr ARI from NOAA Atlas 14, which is not particularly rare considering the overall extreme nature of this storm. Other stations across the domain reported similar tendencies in hourly precipitation, with no particular hour producing an extreme quantity of rainfall. For example, the next three closest observed maximum hourly totals across the domain were 69.85 mm (2.75 in.), 65.28 mm (2.57 in.), and 55.37 mm (2.18 in.), all less than a 10-year ARI according to NOAA Atlas 14 for their respective locations.

Table 1. Maximum 1-, 3-, and 6-h hourly rainfall totals for the 28 hourly stations in the storm domain. 3- and 6-h totals are for single consecutive periods (e.g., 04–06 UTC). Totals with a single asterisk exceeded the NOAA Atlas 14 50-year storm estimate and totals with two asterisks exceed the 200-year estimate.

Station	Station ID	Latitude	Longitude	1-h (mm)	3-h (mm)	6-h (mm)	1-h (in)	3-h (in)	6-h (in)
LAKE CHARLES LA	USW00003937	30.125	-93.2158	77.98	184.66*	298.96**	3.07	7.27*	11.77**
LAFAYETTE RGNL AP LA	USW00013976	30.205	-91.9875	69.85	108.46	145.54	2.75	4.27	5.73
LAFAYETTE 13 SE LA	USW00053960	30.0917	-91.8731	65.28	130.81	134.87	2.57	5.15	5.31
NEW IBERIA ACADIANA RGNL AP LA	USW00053915	30.0375	-91.8839	55.37	99.31	104.14	2.18	3.91	4.1
PORT ARTHUR SE TX AP TX	USW00012917	29.9506	-94.0206	52.58	108.46	176.28	2.07	4.27	6.94
FT. POLK AAF	3931KPOE	31.05	-93.1833	44.2	81.03	94.23	1.74	3.19	3.71
SULPHUR - SOUTHLAND	KUXL	30.1313	-93.3761	42.42	56.64	65.79	1.67	2.23	2.59
HOUSTON INTERCONT AP TX	USW00012960	29.98	-95.36	41.91	58.42	66.8	1.65	2.3	2.63
BATON ROUGE RYAN AP LA	USW00013970	30.5372	-91.1469	39.88	68.07	103.12	1.57	2.68	4.06
GALVESTON SCHOLES FLD TX	USW00012923	29.2733	-94.8592	39.62	48.77	55.37	1.56	1.92	2.18
CONROE MONTGOMERY CO AP TX	USW00053902	30.3567	-95.4139	37.85	51.56	63.5	1.49	2.03	2.5
HOUSTON HOOKS MEM AP TX	USW00053910	30.0675	-95.5561	35.05	68.07	75.69	1.38	2.68	2.98
JENNINGS AWOS	K3R7	30.2427	-92.6735	32.26	36.32	42.67	1.27	1.43	1.68
NEW ORLEANS ALVIN CALLENDER	USW00012958	29.8167	-90.0167	31.24	41.66	44.2	1.23	1.64	1.74
ANGLETON BRAZORIA AP TX	USW00012976	29.1097	-95.4619	30.99	32.51	37.34	1.22	1.28	1.47
ALEXANDRIA ESLER RGNL AP LA	USW00013935	31.3928	-92.2956	28.45	28.96	28.96	1.12	1.14	1.14
ALEXANDRIA INTL AP LA	USW00093915	31.3347	-92.5586	28.45	28.96	28.96	1.12	1.14	1.14
HOUSTON HOBBY AP TX	USW00012918	29.6381	-95.2819	26.67	34.8	45.21	1.05	1.37	1.78
HOUSTON SUGARLAND MEM TX	USW00012977	29.6222	-95.6564	25.91	44.7	51.82	1.02	1.76	2.04
HOUSTON CLOVER FLD TX	USW00012975	29.5189	-95.2417	25.15	35.56	42.16	0.99	1.4	1.66
NEW ORLEANS LAKEFRONT AP LA	USW00053917	30.0494	-90.0289	22.61	28.96	39.37	0.89	1.14	1.55
HUNTSVILLE MUNI AP TX	USW00053903	30.7439	-95.5861	17.78	31.75	38.86	0.7	1.25	1.53
COLLEGE STN TX	USW00003904	30.5892	-96.3647	14.99	37.08	45.97	0.59	1.46	1.81
NEW ORLEANS INTL AP LA	USW00012916	29.9933	-90.2511	14.48	17.27	17.27	0.57	0.68	0.68
LUFKIN ANGELINA CO AP TX	USW00093987	31.2361	-94.7544	8.13	22.86	31.5	0.32	0.9	1.24
MCCOMB/PIKE CO/JOHN E LEWIS AP MS	USW00093919	31.1828	-90.4708	4.32	7.62	13.21	0.17	0.3	0.52
GULFPORT - BILOXI AP MS	USW00093874	30.4119	-89.0808	2.54	4.06	4.32	0.1	0.16	0.17
HATTIESBURG CHAIN MUNI AP MS	USW00013833	31.2819	-89.2531	1.52	2.29	3.56	0.06	0.09	0.14

Of the 28 hourly stations, 6 observed 3-h totals over 76.2 mm (3 in.), mainly around Lake Charles and Lafayette, LA. KLCH reported 184.66 mm (7.27 in.) in 3-h, exceeding the 50-year NOAA Atlas 14 estimate. The next closest 3-h observation was east of Lake Charles in Lafayette, LA (Lafayette 13 SE, LA) with 130.56 mm (5.14 in.), just shy of the NOAA Atlas 14 25-year storm estimate for that location. At the 6-h duration, 6 of the 28 stations observed totals > 101.6 mm (4 in.). At KLCH, 298.96 mm (11.77 in.) of rain was observed in 6-h, exceeding the estimated 200-year frequency estimate for that location. The next closest 6-h total was 176.28 mm (6.94 in.) in Port Arthur, TX, barely exceeding the NOAA Atlas 14 estimated 10-year event.

2. Hourly Gridded Estimates

Since it would be rare for a station (gauge) to observe the maximum accumulated rainfall for a given storm, it is essential to have a tool like SPAS to estimate the storm center location(s) and their total(s). The mass curves for Zone 1 (located just south of Port Arthur, TX; Fig 7) and

Zone 2 (located near Baton Rouge, LA; Fig 8) represent the single highest estimated storm total in each respective Zone, along with estimated hourly accumulations between 01 UTC 16 May–00 UTC 21 May. In Zone 1, SPAS estimated 118.1 mm (4.65 in.) of rain at 14 UTC on 17 May, which is between an estimated 50- (108.7 mm; 4.28 in.) and 100-year (122.17 mm; 4.81 in.) event according to NOAA Atlas 14. In Zone 2, SPAS estimated a lower 1-h maximum value of 75.95 mm (2.99 in) nine hours later, which falls between the estimated 5- (69.1 mm; 2.72 in.) and 10-year (79.25 mm; 3.12 in.) NOAA Atlas 14 estimates for that location. At the 3-h duration, Zone 1 (Zone 2) observed a maximum of 213.11 mm (133.68 mm) of precipitation from 13–15 UTC 17 May (22–00 UTC 17–18 May), which falls between an estimated 100–200-year (10–25-year) event according to NOAA Atlas 14. Finally, at the 6-h duration in Zone 1, SPAS estimated that 295.66 mm (11.64 in.) occurred from 12–17 UTC on 17 May, falling between an estimated 100–200-year event. In Zone 2, 209.4 mm (8.24 in.) occurred from 22–03 UTC spanning 17–18 May, resulting in between a 50–100-year event, according to NOAA Atlas 14.

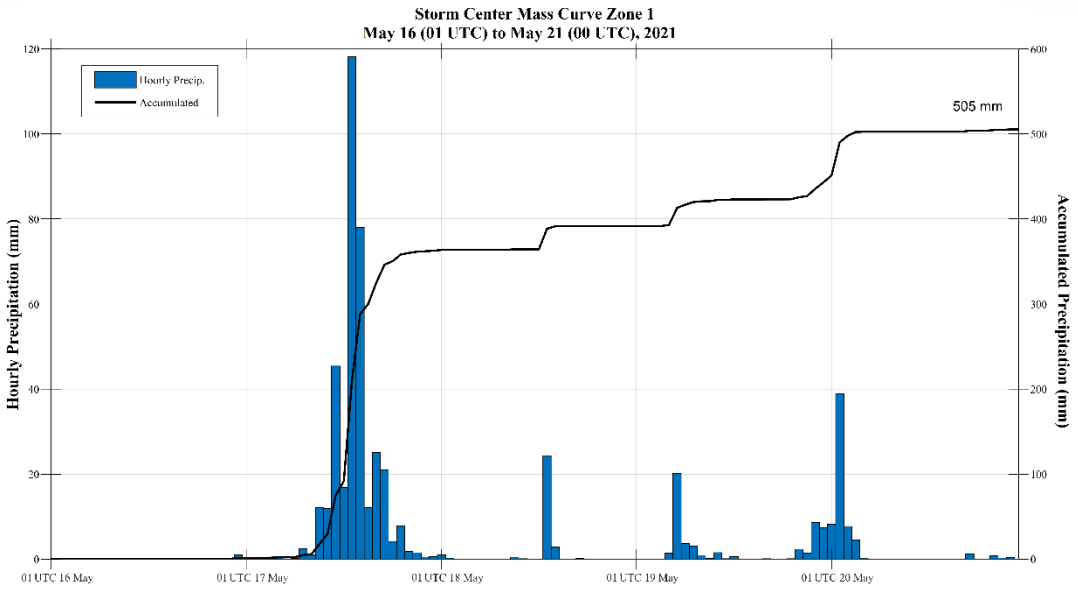

Fig 7. Hourly accumulation and incremental rainfall from 01 UTC 16 May–00 UTC 21 May for the storm center in Zone 1, south of Port Arthur, TX (29.665°N, -93.805°W).

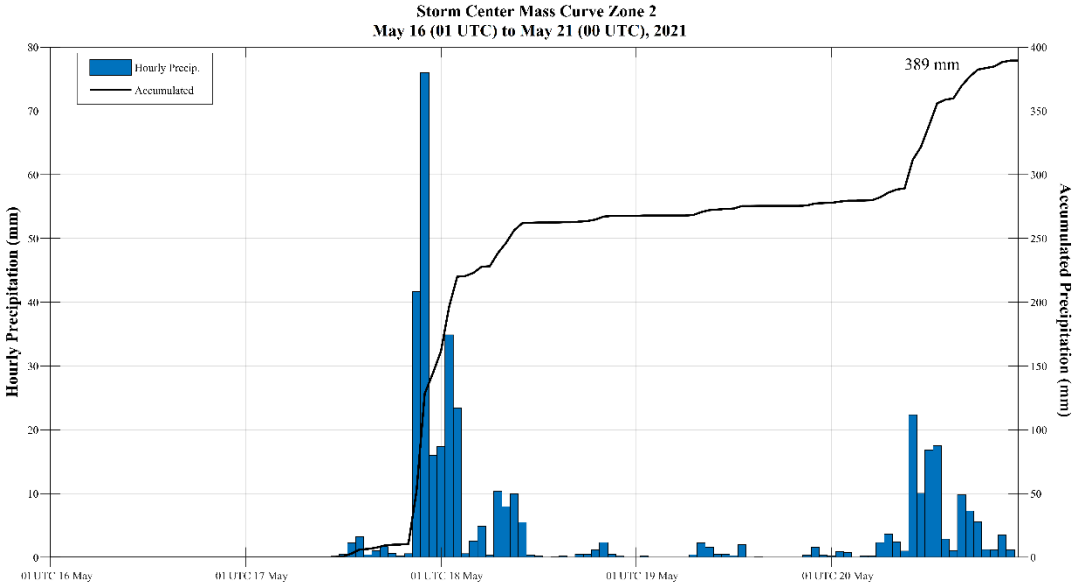

Fig 8. Hourly accumulation and incremental rainfall from 01 UTC 16 May–00 UTC 21 May for the storm center in Zone 2, north of Pierre Part, LA (29.995°N, -91.155°W).

3. 6- and 24- Hour Maximum Rainfall

The above-mentioned hourly rainfall characteristics for Zones 1 and 2 represent the two locations (grid cells) that received (estimated) the greatest 120-h total precipitation during the storm's temporal domain; however, they do not represent the location(s) that received the greatest 1-, 3-, 6-, 12-, or 24-h maximum precipitation amounts. For example, locations just south of Lake Charles, LA, received more precipitation in 6-h than the storm center location in Zone 1. To view sub-total storm durations, storm period maximum rainfall maps (e.g., Fig 9) were produced that estimate the greatest continuous periods (e.g., 01–06 UTC) for each grid cell; however, the date or time of the precipitation may be different for each grid cell (e.g., 6-h max rainfall near Lake Charles, LA did not simultaneously occur with the 6-h max period near Baton Rouge, LA).

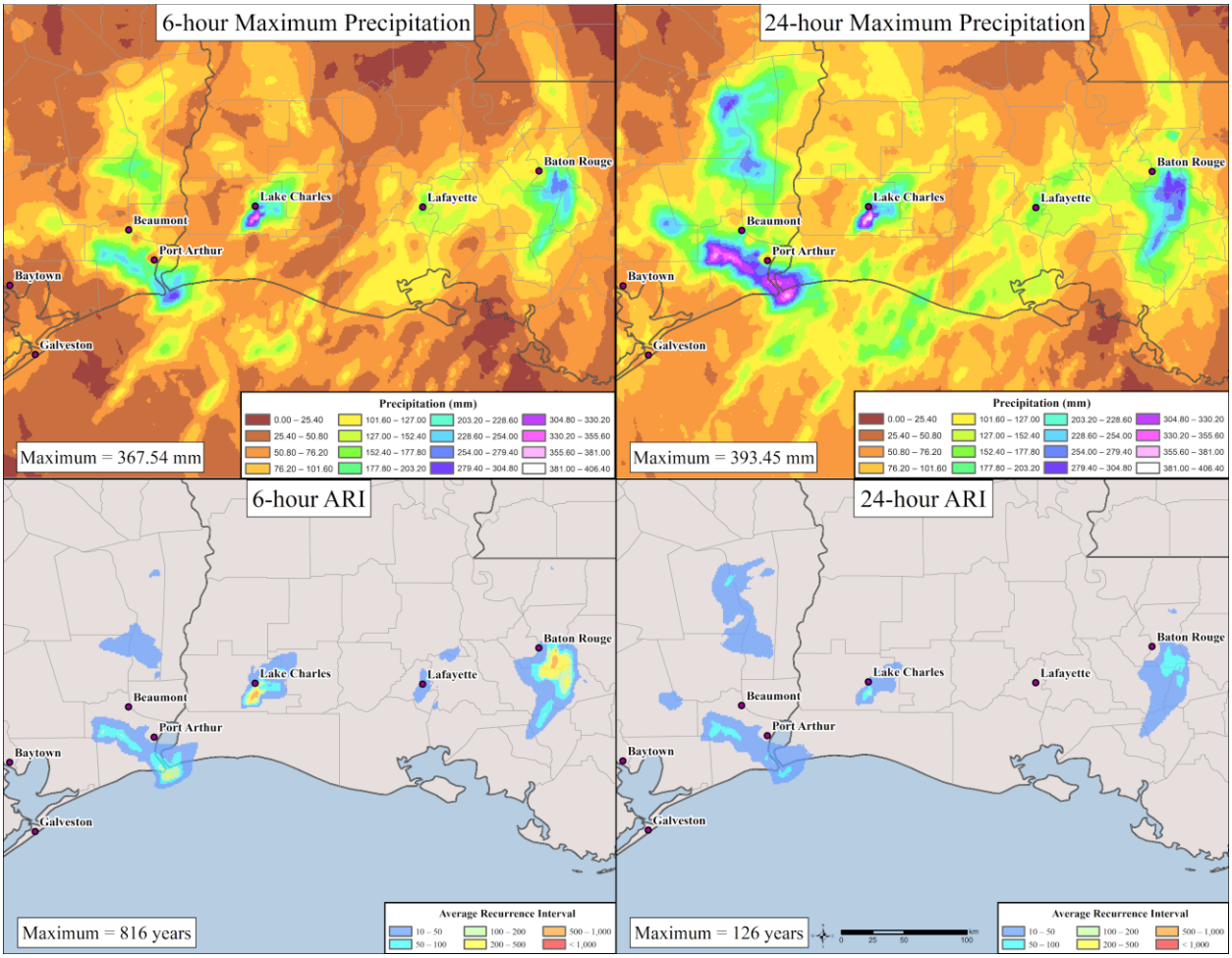

Fig 9. 6-h maximum precipitation (top; left), 6-h annual exceedance probability (bottom; left), 24-h maximum precipitation (top; right), and 24-h annual exceedance probability (bottom; right) for the 16–20 May 2021 event from SPAS.

Figure 9 shows the greatest 6- and 24-h precipitation totals and their corresponding ARI. At the 6-h maximum duration, three distinct areas received notable precipitation. First, South of Port Arthur, TX, where roughly 229–305 mm (9–12 in.) were estimated between 12–17 UTC on 17 May. These totals correspond to roughly a 200–500-year ARI for their respective locations. Second, in Calcasieu Parish, LA, just south of Lake Charles, LA, nearly 254–368 mm (10–14.5 in) is estimated during the 6-h maximum period, from 14–19 UTC on 17 May. These totals surpassed the estimated 200–500-year event, with isolated areas experiencing greater than a 500-year 6 h rainfall total. In fact, a small area roughly 4 km north-northeast of the Lake Charles Regional Airport is estimated to have received 367.5 mm (14.47 in) in 6-h, equating to an ARI of roughly 816-years. Finally, south of Baton Rouge, LA, 203–267 mm (8–10.5 in.) fell in 6-h,

corresponding to ARIs ranging from 200–500-years. Isolated areas near the East Baton Rouge and Iberville Parishes border are estimated to have received 274 mm (10.8 in) between 22–03 UTC spanning 17–18 May, which is roughly a 750-year ARI.

The 24-h maximum period is similar to the storm total (Fig 1) because most of the rainfall that induced flooding occurred in < 24-h (e.g., 6–12 h). Thus, the ARIs for the 24-h period are less extreme, again highlighting how the May 2021 event was primarily a short-duration event. South of Port Arthur in Jefferson County, TX, between 305–368 mm (12–14.5 in) is estimated in 24-h, corresponding to ARIs of 50–100-years. South of Lake Charles, LA, 393.45 mm (15.5 in) was estimated, equivalent to a 126-year ARI, the largest across the storm domain for the period. Finally, just south of Baton Rouge, rainfall totals during the 24-h maximum period were between 279–305 mm (11–12 in), equating ARIs of 50–100-years.

4. Depth-Area-Duration

The maximum depth of precipitation at differing temporal scales was computed for area sizes up to 129,500 km^2 (50,000 mi^2) in Zone 1 (Table 2) and 90,650 km^2 (35,000 mi^2) in Zone 2 (Table 3). Each depth represents the greatest estimated rainfall over a particular area size and duration within the respective Zone (e.g., Fig 3). The values are not necessarily from the storm center location (e.g., Fig 7 and 8), like the 6- and 12-h maximum rainfall discussion above. For each unique duration and area size, SPAS searches within the delineated zone to find the greatest depth of precipitation.

Table 2. Depth–area–duration (DAD) table (mm) for the May 2021 precipitation event (01 UTC 16 May to 00 UTC 21 May) at the storm center in Zone 1, south of Port Arthur, TX (29.665°N, -93.8050°W).

SPAS 1858 - May 16 (0100 UTC) - May 21 (0000 UTC), 2021, Zone 1 MAXIMUM AVERAGE DEPTH OF PRECIPITATION (mm)														
Area (km^2)	Duration (h)													
	1	2	3	4	5	6	12	18	24	36	48	72	96	120
1	95.76	188.72	226.82	295.15	343.66	367.28	384.05	389.89	393.19	406.91	433.58	467.61	467.61	467.61
2.6	94.74	186.69	224.03	291.85	339.85	363.22	379.48	385.57	388.11	402.08	429.01	463.8	464.31	464.31
26	90.17	177.8	213.61	277.88	324.1	346.71	362.71	368.55	369.57	380.75	410.46	453.9	455.42	455.42
65	83.82	162.81	195.58	254.51	296.67	318.26	339.34	351.54	354.84	359.92	386.84	446.53	449.83	449.83
130	81.79	145.8	174.75	227.84	265.94	286.77	327.15	339.09	344.93	348.74	371.86	437.9	441.2	441.2
259	77.98	127.76	153.42	199.64	233.43	256.03	313.69	325.37	332.99	336.55	355.09	420.12	426.72	426.72
389	74.93	120.9	141.99	184.15	215.9	240.28	304.29	315.98	324.1	328.17	343.92	407.42	414.78	414.78
518	74.17	118.11	132.59	177.04	201.93	229.62	296.67	307.85	316.99	321.56	335.53	398.02	406.4	406.4
777	72.39	113.54	125.48	169.93	190.5	215.39	283.97	294.89	304.04	310.9	321.82	384.81	394.46	394.46
1,036	71.12	109.22	121.16	162.81	182.37	204.98	273.81	284.73	293.62	302.26	311.91	372.87	386.08	386.08
1,295	69.85	104.9	116.59	156.21	175.01	197.36	265.18	275.84	283.72	294.13	304.29	361.7	377.7	377.7
2,590	64.01	85.85	99.31	127.76	146.3	169.93	228.6	241.05	251.97	268.22	270.26	322.33	350.27	350.27
5,180	55.88	70.1	78.74	101.09	119.63	132.59	190.75	205.23	218.44	234.44	235.46	284.99	320.8	320.8
9,065	47.5	58.67	67.06	81.79	97.79	105.16	160.27	173.99	185.17	198.37	203.2	254.25	292.61	292.61
12,950	39.12	54.1	63.5	70.1	84.33	91.19	139.7	152.4	162.56	176.02	185.42	235.71	270	270
19,425	29.72	48.26	58.17	63.5	68.33	74.42	116.59	131.06	138.68	151.89	164.85	211.84	244.09	244.09
25,900	25.15	43.94	53.85	59.44	64.01	67.31	101.35	116.33	122.68	136.91	151.13	195.58	224.79	224.79
38,850	21.84	37.85	47.24	52.83	57.15	60.45	84.33	97.54	102.36	116.33	135.38	173.23	199.39	199.39
51,800	19.05	33.27	41.66	47.75	51.82	54.61	71.37	85.85	89.92	102.11	125.73	157.48	180.59	180.59
90,650	11.43	20.57	26.67	32.26	36.32	39.37	49.53	58.17	60.96	73.91	100.08	124.71	143	143
129,500	8.13	14.48	18.8	22.61	26.16	28.45	37.08	44.45	46.48	56.13	77.98	97.28	109.98	109.98

Table 3. Same as Table 2, except for the storm center in Zone 2, north of Pierre Part, LA (29.995°N, -91.155°W).

SPAS 1858 - May 16 (0100 UTC) - May 21 (0000 UTC), 2021, Zone 2 MAXIMUM AVERAGE DEPTH OF PRECIPITATION (mm)														
Area (km^2)	Duration (h)													
	1	2	3	4	5	6	12	18	24	36	48	72	96	120
1	106.68	141.99	182.12	241.3	262.38	276.1	297.69	302.01	303.78	315.47	316.48	316.74	316.74	316.74
2.6	105.92	141.22	181.36	240.03	260.86	274.57	296.42	300.48	302.51	313.69	314.71	314.71	314.71	314.71
26	104.39	138.94	178.82	236.98	257.05	270.51	292.61	296.93	299.21	309.12	309.88	309.88	309.88	309.88
65	103.89	137.92	178.05	235.71	255.78	268.99	291.08	295.4	297.94	307.34	308.1	308.1	308.1	308.1
130	101.6	135.89	174.75	231.65	251.71	264.67	287.27	293.62	296.16	303.02	304.04	304.55	304.55	304.55
259	97.79	131.32	169.16	224.03	243.59	256.03	278.38	284.23	286.77	293.88	294.64	295.15	295.15	295.15
389	93.73	125.73	162.05	214.63	233.17	245.11	266.95	273.3	275.84	282.7	283.72	284.48	284.48	284.48
518	89.15	119.89	154.69	204.72	222.25	233.93	255.52	262.13	264.67	271.78	272.8	273.81	273.81	273.81
777	82.3	111	142.49	188.72	204.72	215.39	237.24	244.35	247.4	254.51	255.52	257.05	257.05	257.05
1,036	76.96	104.65	133.6	177.04	191.52	201.17	223.77	231.9	234.95	241.55	242.82	244.35	244.35	244.35
1,295	72.9	99.57	126.75	168.15	181.61	190.75	212.09	220.47	224.03	230.12	233.43	234.95	234.95	234.95
2,590	60.2	83.82	108.71	142.49	151.89	159	176.02	185.67	189.74	196.09	203.45	206.5	206.5	206.5
5,180	49.02	69.85	93.22	120.65	127.76	133.6	147.57	156.21	160.53	167.89	175.77	179.58	179.58	179.58
9,065	39.88	60.2	82.04	105.92	111.51	116.59	129.03	136.14	140.21	147.07	154.43	159	159	159
12,950	33.78	53.34	74.93	95.5	100.33	104.9	116.59	123.95	128.52	134.87	140.72	145.03	145.03	145.03
19,425	27.18	44.45	63.5	81.03	84.84	88.9	99.31	106.93	111	117.09	122.17	128.78	128.78	128.78
25,900	21.59	37.85	54.1	69.34	73.15	76.2	85.6	92.96	98.81	105.66	109.73	115.82	115.82	115.82
38,850	15.49	26.16	38.61	50.04	52.83	53.85	67.31	75.95	81.28	87.12	90.17	97.03	97.03	97.03
51,800	12.45	20.07	30.23	39.62	41.91	42.16	54.36	62.99	70.87	75.95	78.23	84.07	84.07	84.07
90,650	7.11	12.19	17.78	23.11	24.64	25.4	35.31	41.15	44.96	49.78	50.8	54.61	54.61	54.61

In Zone 1, it is estimated that 95.76 mm (3.77 in.) of rain fell over 1 km^2 in 1-h, less than the estimated total in Zone 2 of 106.9 mm (4.2 in.). In fact, Zone 2 experienced a greater precipitation depth at the 1-h duration for area sizes of 1–1,295 km^2 (0.4–500 mi^2), highlighting the large spatial extent of single-hour totals near Baton Rouge, LA (~13 km east southeast of Louisiana State University). At area sizes between 1–65 km^2 (0.4–25 mi^2) and durations of 2–120 h, Zone 1 has higher estimated depths than Zone 2, corresponding to a small area (< 130 km^2) near Lake Charles, LA, with notable totals. Zone 1 DAD values were greater than Zone 2 for all area sizes at durations longer than 12-h, demonstrating how Zone 2 precipitation was more compressed temporally. In Zone 2, the estimated DAD values were greater than Zone 1 for 1–6 h durations at area sizes of 259–777 km^2 (100–300 mi^2) and 3–5 h durations for 1036–2,590 km^2 (400–1,000 mi^2) area sizes. Thus, Zone 2 precipitation was concentrated in shorter durations (1–6 h). In contrast, Zone 1 had a smaller area with concentrated precipitation (e.g., 178 mm across 26 km^2), while the broader area in Zone 1 experienced greater depths (e.g., Zone 1 had 144 mm more over 96-h at 2,590 km^2).

5. Comparison to August 2016 Southern Louisiana Flood

The August 2016 Southern Louisiana Flood event was a widespread flood disaster that affected Baton Rouge (Wang et al., 2016; Van Der Wiel et al., 2017; Brown et al., 2020a). Here, we compare the August 2016 hybrid/tropical event to the May 2021 event using DAD analysis because both storms impacted a similar area, caused > $1 billion in damages, were analyzed by SPAS enabling easy comparison, and occurred in moist tropical/moderate air masses with elevated (> 90^{th} percentile) precipitable water. It is important to note that the forcing mechanisms of the two events were vastly different. The August 2016 event originated as a tropical wave but, once along the U.S. Gulf Coast, exhibited atypical characteristics of common tropical event definitions (Muller, 1977; Lewis and Keim, 2015; Kunkel and Champion 2019). For example, the storm exhibit a near-uniform horizontal pressure gradient with weak surface winds and exhibited slope with height through the atmosphere rather than a vertically stacked structure typical of tropical events (Brown et al., 2020a).

Figure 10 compares two DAD Zones from the August 2016 Southern Louisiana flood event with the two DAD Zones from the May 2021 event for selected area sizes and durations.

The May 2021 event had greater depths at the 1-h duration for area sizes of 259–2,590 km^2 (100–1,000 mi^2), 2–6 h durations for area sizes of 1–259 km^2 (0.4–100 mi^2), and 2–4 h durations at area sizes of 518–1036 km^2 (200–400 mi^2; not shown). At durations exceeding 12-h, at all area sizes, the August 2016 event had greater precipitation depths. The disparity increased with increasing area size because the May 2021 event was less widespread than the August 2016 event. The differences are most notable at smaller area sizes (e.g., 1–26 km^2) over longer durations (> 12 h); however, the storms were remarkably similar between area sizes of 259–2,590 km^2 (100–1,000 mi^2) at the 1-6 h duration. In terms of application, results from the May 2021 storm are more relevant for relatively small watersheds (< 2,590 km^2) and have rapid precipitation-runoff rates (short times of concentration). The DADs noted here might also be relevant for understanding probable maximum floods (Schreiner and Riedel, 1978; Kappel et al., 2019) across the broader region by demonstrating how much rain is possible over short durations and limited area sizes.

The differences between the DADs, especially at larger area sizes and longer durations, reflect the different meteorological origins of the storms. The disturbance that caused the August 2016 event originated as a tropical wave that drifted (east to west) slowly across the Gulf Coast. The thermodynamic profile of the August 2016 system was much closer to that of a tropical system, exhibiting a warm-core structure with deep, tropical moisture. The record precipitable water value for the New Orleans, LA area (73.62 mm, 2.90 in.) was observed by radiosonde during the August 2016 storm. In contrast, the May 2021 event was driven by a MCVs that stayed just offshore and brought unusually high (but not record-setting) amounts of moisture into the region. Radiosonde observations during the May 2021 storm reveal a thermodynamic environment more like what would be expected during a mid-latitude thunderstorm event. Like tropical systems, the August 2016 event is characterized by consistent hours of unremitting rain over a large area, while the May 2021 event consisted of more isolated thunderstorms concentrated in shorter intervals and over a smaller area.

Despite lower observed precipitable water values, the May 2021 event produced more rainfall over a smaller spatiotemporal extent than the August 2016 event. One potential explanation could be related to precipitation efficiency, as mentioned in the NWS Area Forecast Discussion on 16–17 May 2021. Heavy rainfall events with high efficiency resulting from the

collision-coalescence process need ingredients such as a relatively deep warm-cloud layer (layer from the Lifted Condensation Level (LCL) to the -10°C level), weak/shallow updrafts, limited wind shear, and high relative humidity through a deep layer (Davies, 2001; Ryan and Vitale, 2013). Both events had roughly similar depths below the -10°C isotherm and relatively high humidity, the most important ingredient for precipitation efficiency (Ryan and Vitale, 2013) according to an analysis of skew-T's during the events; however, the May 2021 exhibited less overall CAPE. The May 2021 skew-T's show CAPE concentrated in a thin layer mostly contained at or below -10°C, indicating weak/slow updraft velocity. In this setting, the collision-coalescence process can efficiently grow raindrops before precipitating, indicating excessive rainfall rates, especially in cells with slow movement. This phenomenon can be identified on a skew-T by a thin or narrow CAPE profile (Ryan and Vitale, 2013), like Figures 5 and 6. It is possible the localized, short-duration rainfall produced by the May 2021 event was due to an efficient warm-cloud environment caused by weak updrafts with slow cell motion. Future research will examine the ingredients that enabled the May 2021 to concentrate its rainfall in such a short period and over a relatively small geographic area despite having less precipitable water and CAPE than the August 2016 event.

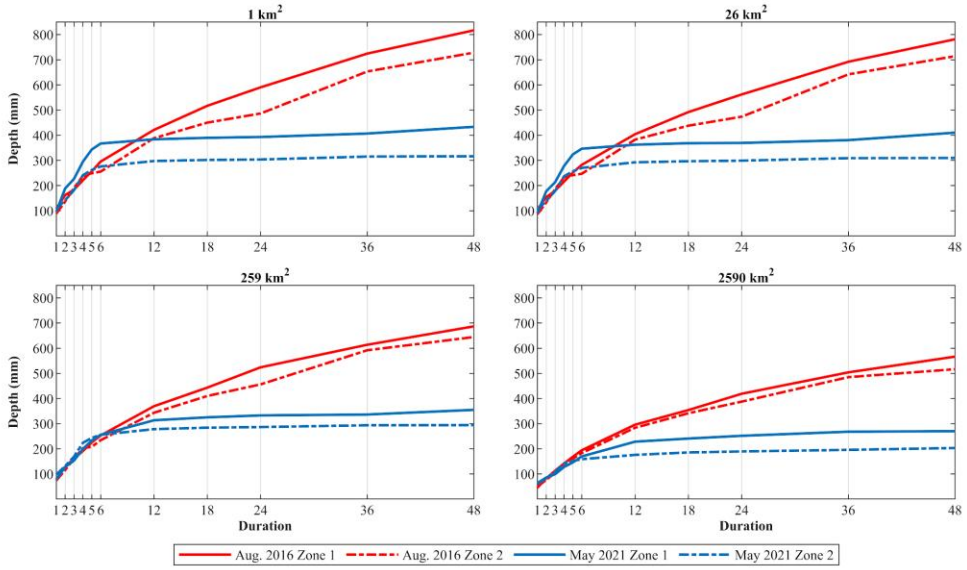

Fig 10. 1-km^2 (0.4-mi^2; top left), 26-km^2 (10-mi^2; top right), 259-km^2 (100-mi^2; bottom; left), and 2,590-km^2 (1,000-mi^2; bottom; right) comparison between the August 2016 Southern Louisiana Flood event (Zone 1 for the Baton Rouge area solid red, Zone 2 for the Lake Charles area dashed red) and the May 2021 event (Zone 1 for the Lake Charles area solid blue, Zone 2 for the Baton Rouge area dashed blue).

4. Discussion and Conclusion

The 16–20 May 2021 extreme rainfall event were related to two mesoscale convective vortices that migrated across southeastern Texas and southern Louisiana. Fed by ample moisture from the Gulf of Mexico, thunderstorms in the complex concentrated precipitation in areas south of Port Arthur, TX, Lake Charles, LA, and Baton Rouge, LA. Using SPAS, it was revealed that a location south of Port Arthur, TX (Zone 1) received an estimated 505 mm (19.88 in.) of rain, while an area farther east, south of Baton Rouge (Zone 2), received 389 mm (15.33 in.) during the storm's precipitation period (01 UTC 16 May–00 UTC 21 May). The May 2021 event's precipitation totals and corresponding ARI across the storm domain during the precipitation period do not accurately represent the unique nature of the storm. For many locations across the storm domain, particularly south of Lake Charles, LA, and Baton Rouge, LA, 50–70% of the storm total occurred in just 6-h, producing ARIs of 200–816-years according to NOAA Atlas 14. At the 24-h duration, precipitation totals were still notable (279–393 mm), but the corresponding ARIs were lower (50–126-years), demonstrating that the storm was focused at the 6-h duration.

A comparison between the May 2021 and August 2016 events was made using DAD analysis. The comparison was of interest because both storms occurred in southern Louisiana, produced > $1 billion in damages, generated remarkable sub-daily totals, and were analyzed by SPAS, enabling easy comparison. Results showed that the May 2021 event exceeded the precipitation depth produced by the August 2016 event at shorter durations and smaller area sizes; however, the storms were remarkably similar at 1–6 h durations and area sizes of 259–2590 km^2. This highlights the efficiency of the precipitation production within the individual convective cells during the May 2021 event and explains the extreme flash flooding caused by this short-lived event. It also rivaled or exceeded the rainfall production of the tropical/hybrid August 2016 event at short durations and small area sizes (e.g., 1–259 km^2). This warrants further research because the August 2016 event had higher observed precipitable water (73.62 mm; record-breaking for KLIX) and contained tropical characteristics yet produced less than or similar precipitation depths at short durations and small area sizes as a non-tropical event with lower observed precipitable water. One potential explanation that will be an area of future research is an efficient precipitation process in slow-moving cells that concentrated across a small area.

The frequency and intensity of extreme precipitation events, such as May 2021 or August 2016, may increase in the future in the absence of moisture limitations or changes in convergence/forcing mechanisms (Sillmann et al., 2013; Wang et al., 2017; Van Oldenborgh et al., 2017; Trenberth et al., 2018, Brown et al. 2019). As the climate continues to warm, precipitation intensity (e.g., the average amount of precipitation per unit time conditional on precipitation falling (Trenberth et al., 2003) will likely increase at a rate near the Clausius–Clapeyron relationship (7% per °C) due to an increase in the atmospheres water vapor capacity (Trenberth, 2011); however, a critical limiting factor for precipitation intensity and extremes, is water vapor availability (Kunkel et al., 2013). For heavy and extreme rainfall, similar to the May 2021 event, moisture must converge via storm-scale circulation from the surrounding area/region (Trenberth et al., 2003). As the climate warms, water vapor increases in the atmosphere (Forster et al., 2021) and studies have shown positive trends in observed surface (Willett et al., 2007) and atmospheric moisture (Santer et al., 2007). In certain conditions (dependent on synoptic setting/storm dynamics), increased water vapor because of a warmer climate may provide more moisture for storms (Scoccimarro et al., 2013), assuming no changes in storm dynamics/convergence, resulting in more frequent heavy rainfall events (Trenberth et al., 2003; Easterling et al., 2017).

While the direct relationship between climate change and individual extreme precipitation events is often difficult to quantify (Kappel, 2019), attribution research (Wang et al., 2016; Van Der Wiel et al., 2017; Van Oldenborgh et al., 2017; Trenberth et al., 2018) and case studies provide a needed understanding of the forcing mechanism and depth of precipitation produced. Future work will continue to expand DAD analysis to define and compare extreme rainfall events to more objectively determine common characteristics and causes that could be related to the changing climate.

Acknowledgments

VMB, BDK, DTT, and AKS would like to acknowledge support from NOAA Grants NA21OAR4310290 and NA21OAR4310306

Data Availability Statement.

All data used in this work is publicly available. Rainfall data are assimilated from six sources Automated Weather Observing Systems, Weather-Bureau-Army-Navy or WBAN, Cooperative Observer Network, Community Collaborative Rain, Hail, & Snow Network, Calcasieu Parish Police Jury's Alert System - One Rain (58 stations), and Jefferson County (Texas) Drainage District No.6. Average recurrence intervals are from NOAA Atlas 14 and 5-min NEXRAD (Level II) Base Reflectivity Mosaics were downloaded from Iowa State University.

References

Brackett, R., 18 May 2021. "Louisiana State of Emergency: Two Dead, One Missing Near Baton Rouge; Hundreds of Lake Charles Homes Damaged." The Weather Channel. Accessed 4 October 2022 https://weather.com/news/news/2021-05-18-louisiana-state-of-emergency-flooding-baton-rouge-lake-charles.

Brown, V.M., Keim, B.D. and Black, A.W., 2019. Climatology and trends in hourly precipitation for the southeast United States. *Journal of Hydrometeorology*, *20*(8), pp.1737–1755. Doi: 10.1175/JHM-D-19-0004.1

Brown, V.M., Keim, B.D., Kappel, W.D., Hultstrand, D.M., Peyrefitte, A.G., Black, A.W., Steinhilber, K.M. and Muhlestein, G.A., 2020a. How rare was the August 2016 South-Central Louisiana heavy rainfall event?. *Journal of Hydrometeorology*, *21*(4), pp.773–790, doi: 10.1175/JHM-D-19-0225.1

Brown, V.M., Keim, B.D. and Black, A.W., 2020b. Trend analysis of multiple extreme hourly precipitation time series in the southeastern United States. *Journal of Applied Meteorology and Climatology*, *59*(3), pp.427–442, doi: 10.1175/JAMC-D-19-0119.1

565 Davis, R.S., 2001. Flash flood forecast and detection methods. In *Severe convective storms* (pp.
566 481–525). Boston, MA: American Meteorological Society.

567 Davies, R., 2 June 2021. "2,700 Homes Damaged in Mid-May Floods in Louisiana, Governor
568 Requests Federal Disaster Declaration." Floodlist. Accessed 10 October 2022 from
569 https://floodlist.com/america/usa/usa-louisiana-governor-requests-federal-disaster-declaration-
570 may-2021-
571 floods#:~:text=The%20state%20government%20of%20Louisiana,weather%20in%20mid%2DM
572 ay%202021.

573 Du, J. 2011. NCEP/EMC 4KM Gridded Data (GRIB) Stage IV Data. Version 1.0. UCAR/NCAR
574 - Earth Observing Laboratory. https://doi.org/10.5065/D6PG1QDD.

575 Easterling, D.R., K.E. Kunkel, J.R. Arnold, T. Knutson, A.N. LeGrande, L.R. Leung, R.S. Vose,
576 D.E. Waliser, and M.F. Wehner, 2017: Precipitation change in the United States. In: Climate
577 Science Special Report: Fourth National Climate Assessment, Volume I [Wuebbles, D.J., D.W.
578 Fahey, K.A. Hibbard, D.J. Dokken, B.C. Stewart, and T.K. Maycock (eds.)]. U.S. Global Change
579 Research Program, Washington, DC, USA, pp. 207–230, doi: 10.7930/J0H993CC.

580 Forster, P., Storelvmo, T., Armour, K., Collins, W., Dufresne, J. L., Frame, D., et al. 2021. The
581 Earth's energy budget, climate feedbacks, and climate sensitivity. In V. Masson-Delmotte, P.
582 Zhai, A. Pirani, S. L. Connors, C. Péan, S. Berger, et al. (Eds.), Climate change 2021: The
583 physical science basis. Contribution of Working Group I to the Sixth Assessment Report of the
584 Intergovernmental Panel on Climate Change. Cambridge University Press.
585 https://doi.org/10.1017/9781009157896.009
586
587 Hultstrand, D. M., and W. D. Kappel, 2017: The Storm Precipitation Analysis System (SPAS)
588 report. Nuclear Regulatory Commission (NRC) Inspection Rep. 99901474/2016-201, Enercon
589 Services, Inc., 95 pp.
590
591 Kappel, W. D., D. M. Hultstrand, J. T. Rodel, G. A. Muhlestein, K. Steinhilber, D. McGlone, J.
592 Rodel, and B. Lawrence, 2015: Statewide probable maximum precipitation for Virginia. Virginia
593 Department of Conservation and Recreation Rep., 129 pp., https://www.dcr.virginia.gov/dam-
594 safety-and-floodplains/document/pmp-final-report.pdf.
595
596 Kappel W.D., and D.M. Hultstrand. 2018: Hurricane Harvey. Journal of Dam Safety, 16(1), 25–
597 34.

Kappel, W. D., 2019: Are storms changing and how does this affect PMP? Dam Safety 2019, Orlando, FL, ASDSO, https://damsafety.org/basic-page/dam-safety-2019-opening-general-session.

Kappel, W. D., D. M. Hultstrand, G. A. Muhlestein, K. Steinhilber, and B. Lawrence, 2019: Regional probable maximum precipitation for the states of Oklahoma, Arkansas, Louisiana, and Mississippi. Tech. Rep., 104 pp., http://www.owrb.ok.gov/damsafety/pdf/2019RegionalPMPStudy.pdf.

Kappel, W.D., Hultstrand, D.M., Rodel, J.T., Muhlestein, G.A., and Steinhilber, K., June 2021: Probable Maximum Precipitation and Annual Exceedance Probability Analysis for the Tittabawassee River Basin, Michigan. Prepared for the Four Lakes Task Force. https://www.four-lakes-taskforce-mi.com/uploads/1/2/3/1/123199575/applied_weather_associates_pmp_study_tittabawassee_river_basin_june_2021.pdf

Kappel, W.D., Hultstrand, D.M., Rodel, J.T., Muhlestein, G.A., Venticinque, M, and Steinhilber, K., December 2021: Site-specific Probable Maximum Precipitation for Antelope Dam, SD. Prepared for DOWL and the Bureau of Indian Affairs.

Kappel, W.D, Hultstrand, D.M., Rodel, J.T., Muhlestein, G.A., Venticinque, M, Cheke, D., and Steinhilber, K., July 2023: Statewide Probable Maximum Precipitation for New Jersey. Prepared for the New Jersey Dept. of Environmental Protection Dam Safety.

Keim, B. D., W. D. Kappel, G. A. Muhlestein, D. M. Hultstrand, T. W. Parzybok, A. B. Lewis, E. M. Tomlinson, and A. W. Black, 2018: Assessment of the extreme rainfall event at Nashville, TN and the surrounding region on May 1–3, 2010. *Journal of the American Water Resources Association, 54*, pp. 1001–1010, doi: 10.1111/1752-1688.12657.

Kelsey, V., Riley, S. and Minschwaner, K., 2022. Atmospheric precipitable water vapor and its correlation with clear-sky infrared temperature observations. *Atmospheric Measurement Techniques*, *15*(5), pp.1563–1576.

Kunkel, K.E., Karl, T.R., Brooks, H., Kossin, J., Lawrimore, J.H., Arndt, D., Bosart, L., Changnon, D., Cutter, S.L., Doesken, N. and Emanuel, K., 2013. Monitoring and understanding trends in extreme storms: State of knowledge. *Bulletin of the American Meteorological Society*, *94*(4), pp.499–514.

636 Kunkel, K.E. and Champion, S.M., 2019. An assessment of rainfall from Hurricanes Harvey and
637 Florence relative to other extremely wet storms in the United States. Geophysical Research
638 Letters, 46(22), pp.13500–13506.
639
640 Kunkel, K.E., Karl, T.R., Squires, M.F., Yin, X., Stegall, S.T. and Easterling, D.R., 2020.
641 Precipitation extremes: Trends and relationships with average precipitation and precipitable
642 water in the contiguous United States. *Journal of Applied Meteorology and Climatology*, *59*(1),
643 pp.125–142.
644
645 Lewis, A.B. and Keim, B.D., 2015. A hybrid procedure for classifying synoptic weather types
646 for Louisiana, USA. International Journal of Climatology, 35(14), pp.4247–4261.
647
648 Lynch, J., Hanna, J., Jackson, A., 19 May 2021. "Louisiana reports at least 4 weather-related
649 deaths as heavy rains deluge state." CNN. Accessed 4 October 2022 from
650 https://www.cnn.com/2021/05/18/weather/flooding-baton-rouge-louisiana-texas/index.html.

651 Latto, A., and Berg, R., 2020. Tropical Storm Imelda. National Hurricane Center Tropical
652 Cyclone Report, 28 pp, https://www.nhc.noaa.gov/data/tcr/AL112019_Imelda.pdf

653 Lehmann, J., Coumou, D. and Frieler, K., 2015. Increased record-breaking precipitation events
654 under global warming. *Climatic Change, 132*, pp.501–515, doi: 10.1007/s10584-015-1434-y.

655 Lincoln, W. S., R. F. Thomason, M. Stackhouse, and D. S. Schlotzhauer, 2017. Utilizing crowd-
656 sourced rainfall and flood impact information to improve the analysis of the North Central Gulf
657 Coast flood event of April 2014. *Journal of Operational. Meteorology*, 5, 26–41,
658 https://doi.org/10.15191/nwajom.2017.0503.

659 Min, S.K., Zhang, X., Zwiers, F.W. and Hegerl, G.C., 2011. Human contribution to more-intense
660 precipitation extremes. *Nature*, *470*(7334), pp.378–381, doi.org/10.1038/nature09763.

661 Muller, R.A., 1977. A synoptic climatology for environmental baseline analysis: New Orleans.
662 Journal of Applied Meteorology (1962-1982), pp.20–33.

663 National Centers for Environmental Information. 2023. Annual 2023 national climate report:
664 National overview. https://www.ncei.noaa.gov/access/monitoring/monthly-
665 report/national/202313.

Parzybok, T. W., and E. M. Tomlinson, 2006: A new system for analyzing precipitation from storms. *Hydro Review*, *25*(3), 58–65.

Parzybok, T.W., Hultstrand, D.M., Tomlinson, E.M. and Kappel, B., 2009, September. Real-time depth-area duration analysis for EAPs and flood warning systems. In *Association of State Dam Safety Officials Annual Conference* (pp. 680–685).

Pasch, R. J., B. J. Reinhart, R. Berg, and D. P. Roberts, 2021: Hurricane Eta. National Hurricane Center Tropical Cyclone Report, 70 pp, https://www.nhc.noaa.gov/data/tcr/AL292020_Eta.pdf

Perica, S., and Coauthors, 2013: Version 2.0: Southeastern States (Alabama, Arkansas, Florida, Georgia, Louisiana, Mississippi). Vol. 9, Precipitation-Frequency Atlas of the United States, NOAA Atlas 14, 163 pp., http://www.nws.noaa.gov/oh/hdsc/PF_documents/Atlas14_Volume9.pdf.

Prein, A.F., Liu, C., Ikeda, K., Trier, S.B., Rasmussen, R.M., Holland, G.J. and Clark, M.P., 2017. Increased rainfall volume from future convective storms in the US. *Nature Climate Change*, *7*(12), pp.880–884.

PRISM Climate Group, Oregon State University, https://prism.oregonstate.edu, data, accessed May 2021.

Santer, B.D., Mears, C., Wentz, F.J., Taylor, K.E., Gleckler, P.J., Wigley, T.M.L., Barnett, T.P., Boyle, J.S., Brüggemann, W., Gillett, N.P. and Klein, S.A., 2007. Identification of human-induced changes in atmospheric moisture content. *Proceedings of the National Academy of Sciences*, *104*(39), pp.15248–15253.

Schreiner, L.C. and Riedel, J.T., 1978. Probable maximum precipitation estimates, United States east of the 105th meridian (No. 51). Department of Commerce, National Oceanic and Atmospheric Administration.

Scoccimarro, E., Gualdi, S., Bellucci, A., Zampieri, M. and Navarra, A., 2013. Heavy precipitation events in a warmer climate: Results from CMIP5 models. *Journal of Climate*, *26*(20), pp.7902–7911, doi: 10.1175/JCLI-D-12-00850.1.

692 Seneviratne, S.I., X. Zhang, M. Adnan, W. Badi, C. Dereczynski, A. Di Luca, S. Ghosh, I.
693 Iskandar, J. Kossin, S. Lewis, F. Otto, I. Pinto, M. Satoh, S.M. Vicente-Serrano, M. Wehner, and
694 B. Zhou, 2021: Weather and Climate Extreme Events in a Changing Climate. In Climate Change
695 2021: The Physical Science Basis. Contribution of Working Group I to the Sixth Assessment
696 Report of the Intergovernmental Panel on Climate Change [Masson-Delmotte, V., P. Zhai, A.
697 Pirani, S.L. Connors, C. Péan, S. Berger, N. Caud, Y. Chen, L. Goldfarb, M.I. Gomis, M. Huang,
698 K. Leitzell, E. Lonnoy, J.B.R. Matthews, T.K. Maycock, T. Waterfield, O. Yelekçi, R. Yu, and
699 B. Zhou (eds.)]. Cambridge University Press, Cambridge, United Kingdom and New York, NY,
700 USA, pp. 1513–1766, doi:10.1017/9781009157896.013.

701 Skeeter, W.J., Senkbeil, J.C. and Keellings, D.J., 2019. Spatial and temporal changes in the
702 frequency and magnitude of intense precipitation events in the southeastern United States.
703 *International Journal of Climatology*, 39(2), pp.768–782.

704 Sillmann, J., Kharin, V.V., Zwiers, F.W., Zhang, X. and Bronaugh, D., 2013. Climate extremes
705 indices in the CMIP5 multimodel ensemble: Part 2. Future climate projections. *Journal of*
706 *Geophysical Research: Atmospheres*, *118*(6), pp.2473–2493, doi: 10.1002/jgrd.50188.

707 Tebaldi, C., Hayhoe, K., Arblaster, J.M. and Meehl, G.A., 2006. Going to the extremes: an
708 intercomparison of model-simulated historical and future changes in extreme events. *Climatic*
709 *Change*, *79*(3-4), pp.185–211, doi: 10.1007/s10584-006-9051-4.

710 Trenberth, K.E., Dai, A., Rasmussen, R.M. and Parsons, D.B., 2003. The changing character of
711 precipitation. *Bulletin of the American Meteorological Society*, *84*(9), pp.1205–1218, doi:
712 10.1175/BAMS-84-9-1205.

713 Trenberth, K.E., 2011. Changes in precipitation with climate change. *Climate Research*, *47*(1-2),
714 pp.123–138, doi: 10.3354/cr00953.

715 Trenberth, K.E., Cheng, L., Jacobs, P., Zhang, Y. and Fasullo, J., 2018. Hurricane Harvey links
716 to ocean heat content and climate change adaptation. *Earth's Future*, *6*(5), pp.730–744, doi:
717 10.1029/2018EF000825.

718 Van Der Wiel, K., Kapnick, S.B., Van Oldenborgh, G.J., Whan, K., Philip, S., Vecchi, G.A.,
719 Singh, R.K., Arrighi, J. and Cullen, H., 2017. Rapid attribution of the August 2016 flood-
720 inducing extreme precipitation in south Louisiana to climate change. *Hydrology and Earth*
721 *System Sciences*, *21*(2), pp.897–921, doi: 10.5194/hess-21-897-2017.

722 Van Oldenborgh, G.J., Van Der Wiel, K., Sebastian, A., Singh, R., Arrighi, J., Otto, F., Haustein,
723 K., Li, S., Vecchi, G. and Cullen, H., 2017. Attribution of extreme rainfall from Hurricane
724 Harvey, August 2017. *Environmental Research Letters*, *12*(12), p.124009, doi: 10.1088/1748-
725 9326/aa9ef2

726 Vitale, J.D. and Ryan, T., 2013. Operational Recognition of High Precipitation Efficiency and
727 Low-Echo-Centroid Convection. *Journal of Operational Meteorology*, *1*(12).

728 WAFB, "Flooding, high-water rescues across metro Baton Rouge," published online May 18,
729 2021. Accessed 4 October 2022 from https://www.wafb.com/2021/05/18/flooding-high-water-
730 rescues-across-metro-baton-rouge/.

731 Wang, R., Fu, Y., Xian, T., Chen, F., Yuan, R., Li, R. and Liu, G., 2017. Evaluation of
732 atmospheric precipitable water characteristics and trends in mainland China from 1995 to
733 2012. *Journal of Climate*, *30*(21), pp.8673–8688.

734 Wang, G., Wang, D., Trenberth, K.E., Erfanian, A., Yu, M., Bosilovich, M.G. and Parr, D.T.,
735 2017. The peak structure and future changes of the relationships between extreme precipitation
736 and temperature. *Nature Climate Change*, *7*(4), pp.268–274.

737 Wang, S.Y.S., Zhao, L. and Gillies, R.R., 2016. Synoptic and quantitative attributions of the
738 extreme precipitation leading to the August 2016 Louisiana flood. *Geophysical Research Letters*,
739 *43*(22), pp.11,805–11,814, doi: 10.1002/2016GL071460.
740
741 Willett, K.M., Gillett, N.P., Jones, P.D. and Thorne, P.W., 2007. Attribution of observed surface
742 humidity changes to human influence. Nature, 449(7163), pp.710–712.